J|A|C|S
ARTICLES
Published on Web 09/27/2006

Energy-Resolved Photoionization of Alkylperoxy Radicals and the Stability of Their Cations

Giovanni Meloni,[†] Peng Zou,[†] Stephen J. Klippenstein,[†,⊥] Musahid Ahmed,[‡] Stephen R. Leone,[‡,§] Craig A. Taatjes,*[,†] and David L. Osborn*[,†]

Contribution from the Combustion Research Facility, Mail Stop 9055, Sandia National Laboratories, Livermore, California 94551-0969, Chemistry Division, Argonne National Laboratory, Argonne, Illinois 60439, Chemical Sciences Division, Ernest Orlando Lawrence Berkeley National Laboratory, Berkeley, California 94720, Departments of Chemistry and Physics, University of California, Berkeley, California 94720

Received June 27, 2006; E-mail: dlosbor@sandia.gov; cataatj@sandia.gov

Abstract: The photoionization of alkylperoxy radicals has been investigated using a newly developed experimental apparatus that combines the tunability of the vacuum ultraviolet radiation of the Advanced Light Source at Lawrence Berkeley National Laboratory with time-resolved mass spectrometry. Methylperoxy (CH_3OO) and ethylperoxy (C_2H_5OO) radicals are produced by the reaction of pulsed, photolytically produced alkyl radicals with molecular oxygen, and the mass spectrum of the reacting mixture is monitored in time by using synchrotron-photoionization with a double-focusing mass spectrometer. The kinetics of product formation is used to confirm the origins and assignments of ionized species. The photoionization efficiency curve for CH_3OO has been measured, and an adiabatic ionization energy of (10.33 ± 0.05) eV was determined with the aid of Franck−Condon spectral simulations, including ionization to the lowest triplet and singlet cation states. Using the appearance energy of CH_3^+ from CH_3OO, an enthalpy of formation for CH_3OO of $\Delta_f H_0^o$ (CH_3OO) = (22.4 ± 5) kJ mol^{-1} is derived. The enthalpy of formation of CH_3OO^+ is derived as $\Delta_f H_0^o$ = (1019 ± 7) kJ mol^{-1} and the CH_3^+-OO bond energy as $D_0^o(CH_3^+ - O_2)$ = (80 ± 7) kJ mol^{-1}. The $C_2H_5OO^+$ signal is not detectable; however, the time profile of the ethyl cation signal suggests its formation from dissociative ionization of C_2H_5OO. Electronic structure calculations suggest that hyperconjugation reduces the stability of the ethylperoxy cation, making the $C_2H_5OO^+$ ground state only slightly bound with respect to the ground-state products, $C_2H_5^+$ and O_2. The value of the measured appearance energy of $C_2H_5^+$ is consistent with dissociative ionization of C_2H_5OO via the Franck−Condon favored ionization to the $\tilde{a}\ ^1A'$ state of $C_2H_5OO^+$.

Introduction

The structure, thermochemistry, and kinetics of alkylperoxy radicals (ROO) have been the subjects of intense study because of these species' central role in reaction processes of societal interest. In particular, ROO radicals are important reaction intermediates in low-temperature oxidation of organic compounds both in the atmosphere, as in the tropospheric "self-cleansing" mechanism to remove volatile organic compounds,[1,2] and in combustion, especially in autoignition chemistry.[3−5] In the earth's atmosphere, alkyl radicals (R) are formed in the oxidation of saturated hydrocarbons (RH) with strong oxidizers such as NO_3 [6]

$$RH + NO_3 \rightarrow R + HNO_3 \quad (1)$$

or OH[7,8]

$$RH + OH \rightarrow R + H_2O \quad (2)$$

The alkyl radicals can then add O_2 via a three-body reaction,

$$R + O_2 + M \rightarrow ROO + M \quad (3)$$

During combustion processes, ROO radicals are also produced by the addition of alkyl radicals to O_2. However, depending on the temperature regime, the ROO can lead to different products. The hydroperoxyalkyl radical isomerization product of internal hydrogen abstractions, often denoted QOOH, is responsible for

[†] Sandia National Laboratories.
[⊥] Argonne National Laboratory.
[‡] Ernest Orlando Lawrence Berkeley National Laboratory.
[§] University of California.

(1) Carter, W. P. L. *Atmos. Environ. A* **1990**, *24*, 481−518.
(2) Atkinson, R.; Baulch, D. L.; Cox, R. A.; Hampson, R. F.; Kerr, J. A.; Rossi, M. J.; Troe, J. *J. Phys. Chem. Ref. Data* **1997**, *26*, 521−1011.
(3) Benson, S. W. *J. Am. Chem. Soc.* **1965**, *87*, 972−979.
(4) Cox, R. A.; Cole, J. A. *Combust. Flame* **1985**, *60*, 109−123.
(5) Pilling, M. J.; Robertson, S. H.; Seakins, P. W. *J. Chem. Soc., Faraday Trans.* **1995**, *91*, 4179−4188.
(6) Platt, U.; Lebras, G.; Poulet, G.; Burrows, J. P.; Moortgat, G. *Nature* **1990**, *348*, 147−149.
(7) Lightfoot, P. D.; Cox, R. A.; Crowley, J. N.; Destriau, M.; Hayman, G. D.; Jenkin, M. E.; Moortgat, G. K.; Zabel, F. *Atmos. Environ. A* **1992**, *26*, 1805−1961.
(8) Madronich, S.; Greenberg, J.; Paulson, S. *Atmospheric Chemistry and Global Change*, 1st ed.; Oxford University Press: New York, 1999; p 325.

10.1021/ja064556j CCC: $33.50

the low-temperature chain branching implicated in engine knock, one of the limiting factors on the efficiency of internal combustion engines.[9]

In general, ROO radicals are only moderately reactive toward other molecules except for odd-electron species such as radicals or nitrogen oxides. In this regard, an important atmospheric process is the reaction with nitric oxide to produce tropospheric ozone.[7,10,11]

$$ROO + NO \rightarrow RO + NO_2 \quad (4)$$

$$NO_2 + h\nu \rightarrow NO + O\,(^3P) \quad (5)$$

$$O_2 + O\,(^3P) + M \rightarrow O_3 + M \quad (6)$$

These reactions are part of the photochemical smog cycle. Alkylperoxy radicals are also key intermediates in the heterogeneous oxidation of hydrocarbons on aerosol surfaces, where the abstraction of H atoms from a hydrocarbon at the surface and subsequent reaction with O_2 produces surface-bound ROO radicals.[12,13] Furthermore, in living organisms alkylperoxy radicals are initiators and chain propagators of autoxidation processes relevant to oxidative damage to polyunsaturated fatty acids.[14,15] The thermochemistry of ROO species, and the possibility of monitoring them by photoionization, is relevant to many areas of chemistry.

Methyl- and ethylperoxy radicals have been extensively investigated employing ab initio and density functional methods by many groups, such as Bair and Goddard,[16] Lin and co-workers,[17] and Jafri and Phillips[18] for CH_3OO; and Miller and Klippenstein,[19,20] Schaefer and co-workers[21−23] and Okumura and co-workers[24] for C_2H_5OO, leading to optimized geometries, vibrational frequencies, dissociation energies, relative stability of different isomers, and potential energy surfaces. Much of the experimental knowledge of the thermochemistry of ROO radicals is derived from reaction kinetics[25,26] or from negative ion spectroscopy.[24,27] Despite the significance of ROO radicals in combustion and atmospheric chemistry, the ionization energies of alkylperoxy radicals have not been determined, and the stability of their cations has not previously been experimentally investigated. The methylperoxy cation CH_3OO^+ has been produced by electron impact ionization[28] and photoionization with an Ar resonance lamp (11.62 and 11.83 eV);[25,29] detection of higher peroxy radical cations has proved difficult. The inability to detect larger ROO radicals by photoionization has been suggested to arise simply because of low photoionization cross sections.[30,31] Very recently (while this article was in review), Bernstein and co-workers[32] measured photoionization at 10.5 eV of several peroxy radicals in a supersonic jet. They observed only dissociative ionization, i.e., a fragmentation of the parent to a daughter cation, a neutral, and an electron, for ethylperoxy and propylperoxy radicals and presented density functional calculations that suggested the ethylperoxy and propylperoxy cations are unstable. The present work corroborates the view that it is the instability of the cation that has prevented observation of the photoionization and that the competition between parent ionization and dissociative ionization is key to the study of alkylperoxy photoionization. Additionally, knowledge of photoionization processes in ROO radicals has important implications for direct monitoring of alkylperoxy radicals by ionization methods, either in a laboratory or field environment.

This work presents the first experimental determination of the ionization energy of CH_3OO, measured using a new experimental apparatus that combines single-photon ionization with a time- and photon-energy-resolved mass spectrometer. This new instrument allows monitoring the formation and depletion of multiple chemical species during photolytically initiated reactions. We present the photoionization efficiency (PIE) curve of the CH_3OO radical, which undergoes direct ionization, and the appearance energy curve of the $C_2H_5^+$ fragment from the dissociative ionization of C_2H_5OO. The appearance energy of CH_3^+ from CH_3OO is also derived. The results are analyzed with the aid of electronic structure calculations and Franck−Condon (FC) spectral simulations, and inferences on the stability of the corresponding cations are discussed. The reduced stability of the $C_2H_5OO^+$ ion is largely attributable to the stabilizing effects of hyperconjugation on the alkyl cation fragment, an effect that should be generally relevant to larger alkyl peroxy cations.

Experimental Section

Apparatus. The recently constructed experimental apparatus used in this work will be described in detail in a future publication. The instrument is designed to investigate the kinetics of elementary gas-phase reactions by monitoring the time-resolved concentrations of multiple chemical species following initiation of chemical reaction by pulsed laser photolysis. Schematically illustrated in Figure 1, it consists of a slow-flow reactor (following the Slagle and Gutman design),[25] in which reactions are photolytically initiated, coupled to a multiplexed photoionization mass spectrometer. Mass flow controllers deliver the photolytic precursor (e.g., acetone) and an excess reactant (O_2) in a large excess of helium to the flow tube reactor, a 60 cm long, straight quartz tube with 1.05 cm inner diameter. This gas mixture moves down the flow tube at a velocity of ~400 cm s^{-1} toward a vacuum pump throttled by a valve that regulates the tube pressure under active

(9) Westbrook, C. K. *Chem. Ind.* **1992** (15), 562−566.
(10) Wallington, T. J.; Dagaut, P.; Kurylo, M. J. *Chem. Rev.* **1992**, *92*, 667−710.
(11) Finlayson-Pitts, B. J.; Pitts, J. N. *Science* **1997**, *276*, 1045−52.
(12) Bertram, A. K.; Ivanov, A. V.; Hunter, M.; Molina, L. T.; Molina, M. J. *J. Phys. Chem. A* **2001**, *105*, 9415−9421.
(13) Nandi, S.; Blanksby, S. J.; Zhang, X.; Nimlos, M. R.; Dayton, D. C.; Ellison, G. B. *J. Phys. Chem. A* **2002**, *106*, 7547−7556.
(14) Jovanovic, S. V.; Jankovic, I.; Josimovic, L. *J. Am. Chem. Soc.* **1992**, *114*, 9018−9021.
(15) Ames, B. N. *Science* **1983**, *221*, 1256−1264.
(16) Bair, R. A.; Goddard, W. A. *J. Am. Chem. Soc.* **1982**, *104*, 2719−2724.
(17) Zhu, R.; Hsu, C. C.; Lin, M. C. *J. Chem. Phys.* **2001**, *115*, 195−203.
(18) Jafri, J. A.; Phillips, D. H. *J. Am. Chem. Soc.* **1990**, *112*, 2586−90.
(19) Miller, J. A.; Klippenstein, S. J. *Int. J. Chem. Kinet.* **2001**, *33*, 654−668.
(20) Miller, J. A.; Klippenstein, S. J.; Robertson, S. H. *Proc. Combust. Inst.* **2000**, *28*, 1479−1486.
(21) Quelch, G. E.; Gallo, M. M.; Schaefer, H. F. *J. Am. Chem. Soc.* **1992**, *114*, 8239−8247.
(22) Quelch, G. E.; Gallo, M. M.; Shen, M. Z.; Xie, Y. M.; Schaefer, H. F.; Moncrieff, D. *J. Am. Chem. Soc.* **1994**, *116*, 4953−4962.
(23) Rienstra-Kiracofe, J. C.; Allen, W. D.; Schaefer, H. F. *J. Phys. Chem. A* **2000**, *104*, 9823−9840.
(24) Blanksby, S. J.; Ramond, T. M.; Davico, G. E.; Nimlos, M. R.; Kato, S.; Bierbaum, V. M.; Lineberger, W. C.; Ellison, G. B.; Okumura, M. *J. Am. Chem. Soc.* **2001**, *123*, 9585−9596.
(25) Slagle, I. R.; Gutman, D. *J. Am. Chem. Soc.* **1985**, *107*, 5342−5347.
(26) Knyazev, V. D.; Slagle, I. R. *J. Phys. Chem. A* **1998**, *102*, 1770−1778.
(27) Clifford, E. P.; Wenthold, P. G.; Gareyev, R.; Lineberger, W. C.; DePuy, C. H.; Bierbaum, V. M.; Ellison, G. B. *J. Chem. Phys.* **1998**, *109*, 10293−10310.
(28) Plumb, I. C.; Ryan, K. R.; Steven, J. R.; Mulcahy, M. F. R. *J. Phys. Chem.* **1981**, *85*, 3136−3138.
(29) Washida, N.; Bayes, K. D. *Int. J. Chem. Kinet.* **1976**, *8*, 777−794.
(30) McDade, C. E.; Lenhardt, T. M.; Bayes, K. D. *J. Photochem.* **1982**, *20*, 1−7.
(31) Wu, D.; Bayes, K. D. *Int. J. Chem. Kinet.* **1986**, *18*, 547−554.
(32) Fu, H. B.; Hu, Y. J.; Bernstein, E. R. *J. Chem. Phys.* **2006**, *125*, 014310.

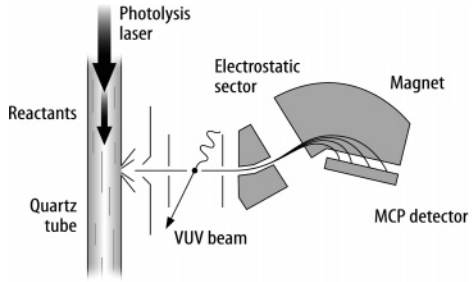

Figure 1. Schematic of the experimental apparatus (see text for details).

feedback control. In the present experiments, acetone (>99.5% purity), 3-pentanone (diethyl ketone) (>99%), and 5-heptanone (98%) are used as precursors for CH_3, C_2H_5 and n-C_3H_7 radicals, respectively. Samples are degassed either by repeated freeze−pump−thaw cycles, or by bubbling helium for several hours through the ketone.

The beam of an unfocused, 4 Hz repetition rate ArF excimer laser (193.3 nm) with a 20 ns pulse width propagates down the tube, photodissociating the precursor species with a fluence of between 10 and 25 mJ cm^{-2} $pulse^{-1}$. A uniform density of radicals (e.g., CH_3) is thus created along the length of the tube. Chemical reactions proceed uniformly along the length of the reactor as the irradiated plug of gas moves down the tube. The flow velocity is sufficient to sweep a fresh sample of gas into the tube before the next photodissociation laser pulse. Gas is extracted from the flow tube through a 600 μm diameter pinhole in the side of the tube, located 35 cm downstream from the tube entrance, into a chamber pumped by a 3200 L s^{-1} turbomolecular pump. The effusive beam emerging from the pinhole is skimmed by a 1.5 mm diameter skimmer before entering a differentially pumped ionization region.

The gas beam is crossed in the ionization region by synchrotron undulator radiation that has been dispersed by a 3 m monochromator at the Chemical Dynamics Beamline of the Advanced Light Source at Lawrence Berkeley National Laboratory. A gas filter with Ar at 30 Torr is placed in the beamline to suppress undulator harmonics at higher energy. The quasi-continuous, tunable vacuum ultraviolet light from the synchrotron ionizes molecules from the reactor within the ionization region of a miniature double-focusing magnetic-sector mass spectrometer of the Mattauch−Herzog geometry.[33] Ions are accelerated, focused, and dispersed according to the square root of their mass in a 0.94 T magnetic field. At the exit plane of the magnet, all ions within a variable mass range of 6 × (e.g., m/z = 14 to 84) strike the active area of a time- and position-sensitive microchannel plate detector with a delay-line anode.[34] The position and time of arrival with respect to the photodissociation laser is recorded for each ion. The experiment is repeated, and the signal averaged, for up to 20000 laser pulses.

The photon energy of the synchrotron can be scanned during an acquisition, yielding a complete series of time-resolved mass spectra at each photoionization energy. The photon energy ($h\nu_{ALS}$) and the energy resolution (40 meV for 600 μm exit slit width, 80 meV for 1 mm slit width) are calibrated by measurement of known atomic resonances of Xe, absorption resonances of Ar (using the gas filter as an absorption cell), and narrow autoionization resonances in O_2. Further confirmation of the energy calibration is made during the measurements of CH_3OO photoionization by measurement of the ionization threshold of acetone.[35]

Because the apparatus collects time- and photon-energy-resolved mass spectra, a three-dimensional data block is available for each experiment containing ion intensity as a function of mass-to-charge ratio, reaction time, and photon energy. Figure 2 depicts one two-dimensional (2D) section of this three-dimensional (3D) data, showing the time-resolved mass spectrum for the reaction of CH_3 with O_2 taken at a photon energy of 11 eV. Because the focus of this work is on identification and characterization of the product ROO species, the oxygen concentrations are chosen so that the initial addition to form ROO is rapid. Secondary reactions of the ROO and other radical species are slow enough that they can be readily distinguished from the primary process on the basis of the kinetic profile. The photoionization efficiency (PIE) curve is constructed by integrating the three-dimensional data first over the desired mass-to-charge ratio, then over a time window that corresponds to the production of the species of interest in the photolytically initiated reaction. Background contributions at the same m/z are removed by subtraction of a similarly integrated signal taken before the photodissociation laser is fired. Finally, this background-subtracted signal at each photon energy is normalized for the ALS photon current and accumulated into the PIE spectrum.

Electronic Structure Calculations. Molecular parameters, energetics, and force constants of the CH_3OO/CH_3OO^+ and $C_2H_5OO/C_2H_5OO^+$ species are calculated using the Gaussian03 program package.[36] The Becke three-parameter exchange functional with the Lee, Yang, and Parr correlation functional (B3LYP) method and Dunning's augmented cc-pVTZ basis set is employed for geometry optimizations and anharmonic frequency analyses used in the Franck−Condon simulations. Higher-level estimates of total energies (including zero-point energies) are computed with two different methods. The first method was the complete basis set (CBS) method of Petersson and co-workers using the atomic pair natural orbital (APNO) expansion.[37,38] This method approximates energies at the QCISD(T)/CBS level of theory with geometries optimized at the QCISD/6-311G(d,p) level, providing thermochemical values with mean absolute deviation from experiment of 2 kJ mol^{-1} for a reference set of molecules. Additionally, QCISD(T) calculations for the cc-pVTZ and cc-pVQZ basis sets were extrapolated to the complete basis set limit. The latter calculations, which are labeled QCISD(T)/∞ here, employed B3LYP/6-311++G-(d,p) geometries and have been shown in related studies[39−41] to yield very good agreement with observed ionization energies for a number of molecules and radicals. The energetics are summarized in Table 1, and the molecular parameters are shown in Table 2. These two methods are expected to give results that are accurate to within 5 to 10 kJ mol^{-1}

It is known that theoretical methods do not give reliable predictions for severely spin-contaminated wave functions.[42] For all states presented in Table 1, the expectation value of $\langle S^2 \rangle$ indicates negligible spin contamination. The Q1 diagnostic,[43] for which values greater than 0.02 are indicative of significant multireference character, is also reported in Table 1. For many of the species, this diagnostic is somewhat greater than 0.02, but never by very much, and so the QCISD(T) calculated energies should be fairly reliable. All frequencies are found to be real, indicating that our geometries represent minima on the potential surface.

In the $\tilde{X}\,^2A''$ ground states of both CH_3OO and C_2H_5OO, the unpaired electron occupies the out-of-plane 2p-like orbital of the terminal oxygen (perpendicular to the H−C−O−O plane), whereas in the low-lying

(33) Sinha, M. P.; Wadsworth, M. *Rev. Sci. Instrum.* **2005**, *76*, 025103−025108.
(34) Vallerga, J. V.; Siegmund, O. H. W. *Nucl. Inst. Methods Phys. Res. A* **2000**, *442*, 159−163.
(35) Trott, W. M.; Blais, N. C.; Walters, E. A. *J. Chem. Phys.* **1978**, *69*, 3150−3158.
(36) Frisch, M. J.; et al. *Gaussian 03*, revision C.02; Gaussian, Inc.: Wallingford, CT, 2004.
(37) Montgomery, J. A.; Ochterski, J. W.; Petersson, G. A. *J. Chem. Phys.* **1994**, *101*, 5900−5909.
(38) Ochterski, J. W.; Petersson, G. A.; Montgomery, J. A. *J. Chem. Phys.* **1996**, *104*, 2598−2619.
(39) Taatjes, C. A.; Klippenstein, S. J.; Hansen, N.; Miller, J. A.; Cool, T. A.; Wang, J.; Law, M. E.; Westmoreland, P. R. *Phys. Chem. Chem. Phys.* **2005**, *7*, 806−813.
(40) Hansen, N.; Klippenstein, S. J.; Taatjes, C. A.; Miller, J. A.; Wang, J.; Cool, T. A.; Yang, B.; Yang, R.; Wei, L.; Huang, C.; Wang, J.; Qi, F.; Law, M. E.; Westmoreland, P. R. *J. Phys. Chem. A* **2006**, *110*, 3670−3678.
(41) Hansen, N.; Klippenstein, S. J.; Miller, J. A.; Wang, J.; Cool, T. A.; Law, M. E.; Westmoreland, P. R.; Kasper, T.; Kohse-Höinghaus, K. *J. Phys. Chem. A* **2006**, *110*, 4376−4388.
(42) Mayer, P. M.; Parkinson, C. J.; Smith, D. M.; Radom, L. *J. Chem. Phys.* **1998**, *108*, 604−15.
(43) Lee, T. J.; Rendell, A. P.; Taylor, P. R. *J. Phys. Chem.* **1990**, *94*, 5463−5468.

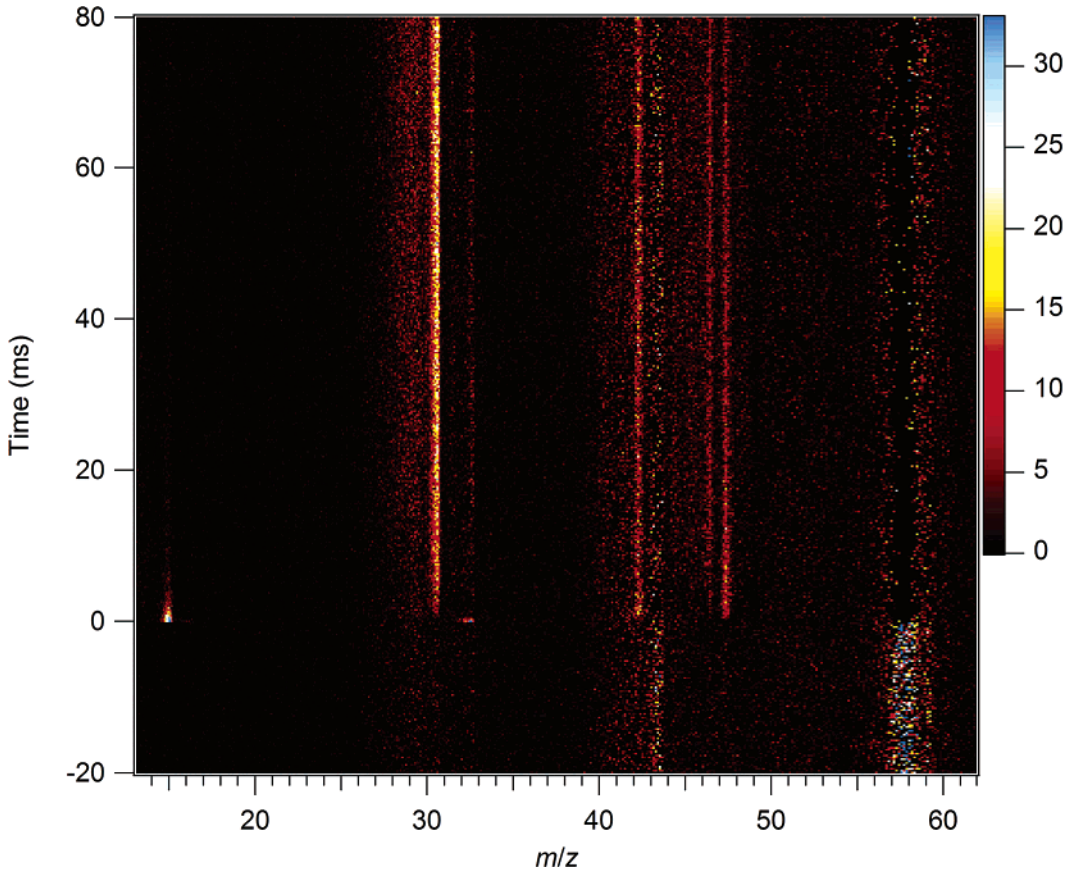

Figure 2. Time-resolved mass spectrum for the reaction of CH_3 with O_2 taken at a photon energy of 11 eV.

Table 1. Energies for CH_3OO and C_2H_5OO[a]

species	state	energy (eV) CBS-APNO	QCISD(T)/∞[b]	Q1[c]
CH_3OO	$\tilde{X}\ ^2A''$	0	0	0.032
	$\tilde{A}\ ^2A'$	0.92		
CH_3OO^+	$\tilde{X}\ ^3A''$	10.21	10.26	0.032
	$\tilde{a}\ ^1A'$	10.43	10.38	0.022
C_2H_5OO	$\tilde{X}\ ^2A''$	0	0	0.032
	$\tilde{A}\ ^2A'$	0.92		
$C_2H_5OO^+$	$\tilde{X}\ ^3A''$	9.48	9.58	0.026
	$\tilde{a}\ ^1A'$	10.06	10.01	0.021
$C_2H_5^+ + O_2$	$^1A_1$, $^3\Sigma_g^-$	9.56	9.55	0.010, 0.014

[a] All energies include zero-point corrections. For CH_3OO species the energies are relative to the ground state of CH_3OO, and for C_2H_5OO energies are relative to the ground state of C_2H_5OO. [b] Energies evaluated at the B3LYP/6-311++G** geometry. [c] Q1 diagnostic from QCISD(T) calculations.

$\tilde{A}\ ^2A'$ excited state the unpaired electron occupies the in-plane 2p-like orbital of the terminal oxygen. A schematic potential energy surface diagram as a function of the R−OO bond distance that maintains C_s symmetry is shown in Figure 3 for CH_3OO/CH_3OO^+ and Figure 4 for $C_2H_5OO/\ C_2H_5OO^+$. Note that the ROO $\tilde{A}\ ^2A'$ states correlate within C_s symmetry to R + O_2 ($a\ ^1\Delta$), whereas the ROO $\tilde{X}\ ^2A''$ states correlate with R + O_2 ($X\ ^3\Sigma_g^-$).

Results and Discussion

CH_3OO. The experimental CH_3OO photoionization efficiency curve, shown in Figure 5, presents a distinct onset at ~10.3 eV with a gradual threshold. No individual vibrational thresholds are observed. To analyze these data, we simulate the PIE curve of CH_3OO using Franck−Condon calculations based on a set of computed optimized geometries, vibrational frequencies, and force constants for the neutral and cation states from the B3LYP/aug-cc-pVTZ calculations. All eight totally symmetric vibrational modes of CH_3OO are included in the simulations. Four of these modes show substantial displacement upon photoionization. The most active mode is ν_2, corresponding to COO bending, owing to a change of 10° in the $\angle C_\alpha OO$ angle between the $\tilde{X}\ ^2A''$ and $\tilde{X}\ ^3A''$ states and 7° between the $\tilde{X}(^2A'')$ and $\tilde{a}\ ^1A'$ (see Table 2). The computed ν_2 wavenumber of 493 cm^{-1} for the neutral ground state is in good agreement with the experimental value of (482 ± 9) cm^{-1} from Blanskby et al.[24] in a negative ion photoelectron spectroscopy study and 492 cm^{-1} from Nandi et al.[13] in a FTIR cryogenic matrix isolation investigation.

The simulated PIE curve is generated by computation and integration of the photoelectron (PE) spectrum of CH_3OO. The PE simulation was carried out within the Franck−Condon (FC) approximation using the PESCAL program,[44,45] which includes treatment of Duschinsky rotation.[46] The simulated CH_3OO PIE curve is shown in Figure 5, superimposed on the experimental PIE curve. Adiabatic ionization energies (AIE) are often estimated from the midpoint rise of a clear vibrational threshold in a photoionization efficiency spectrum. In the case of CH_3OO, no sharp threshold is observed, and the present determination for the AIE of (10.33 ± 0.05) eV for the adiabatic ionization energy of the $\tilde{X}\ ^2A''$ state is based on a fit of the experimental PIE curve to a sum of the Franck−Condon envelopes for ionization to the singlet and triplet cation states.

(44) Ervin, K. M.; Ramond, T. M.; Davico, G. E.; Schwartz, R. L.; Casey, S. M.; Lineberger, W. C. *J. Phys. Chem. A* **2001**, *105*, 10822−10831.
(45) Ervin, K. M. *PESCAL*, Fortran program, 2004.
(46) Duschinsky, F. *Acta Physicochim. URSS* **1937**, *7*, 551

Table 2. Bond Distances (Å) and Angles (deg) Optimized at the B3LYP/aug-cc-pVTZ Level of Theory[a]

molecule	$r_{C_\beta-H}$	$r_{C_\alpha-H}$	$r_{C_\alpha-C_\beta}$	$r_{C_\alpha-O}$	r_{O-O}	$\angle C_\alpha OO$	$\angle HCH$	θ^b
$\tilde{X}\,^2A''$**CH_3OO**		1.09		1.44	1.32	111	111	180
$\tilde{A}\,^2A'$**CH_3OO**		1.09		1.44	1.38	108	110	180
$\tilde{X}\,^3A''$**CH_3OO^+**		1.08		1.65	1.20	121	116 ($H_\alpha C_\alpha H$)	180
							117 ($HC_\alpha H$)	
$\tilde{a}\,^1A'$ **CH_3OO^+**		1.08[c]		1.48	1.20	118	116 ($H_\alpha C_\alpha H$)	0
		1.09					108 ($HC_\alpha H$)	
$\tilde{X}\,^2A''$**C_2H_5OO**	1.09[d]	1.08	1.51	1.46	1.31	112	109 ($HC_\alpha H$)	180
	1.09						109 ($HC_\beta H$)	
$\tilde{A}\,^2A'$**C_2H_5OO**	1.09[d]	1.09	1.51	1.44	1.38	108	109 ($HC_\alpha H$)	180
	1.09						109 ($HC_\beta H$)	
$\tilde{X}\,^3A''$**$C_2H_5OO^+$**	1.12[d]	1.08	1.42	2.18	1.20	123	117 ($HC_\alpha H$)	180
	1.09						115 ($HC_\beta H$)	
$\tilde{a}\,^1A'$ **$C_2H_5OO^+$**	1.09[d]	1.10	1.47	1.50	1.20	118	105 ($HC_\alpha H$)	0
	1.09						109 ($HC_\beta H$)	

[a] The C atom attached to the OO is denoted as C_α, and the other C atom in C_2H_5OO as C_β. [b] θ is the dihedral angle formed by the $H_\alpha-C_\alpha-O-O$ (for CH_3OO) or $C_\beta-C_\alpha-O-O$ (for C_2H_5OO) bonds. [c] This $r_{C_\alpha-H}$ is the bond length between the C_α and the H (H_α) lying in the C−O−O plane. [d] This $r_{C_\beta-H}$ is the bond length between the C_β and the H (H_β) lying in the $C_\beta-C_\alpha-O-O$ plane.

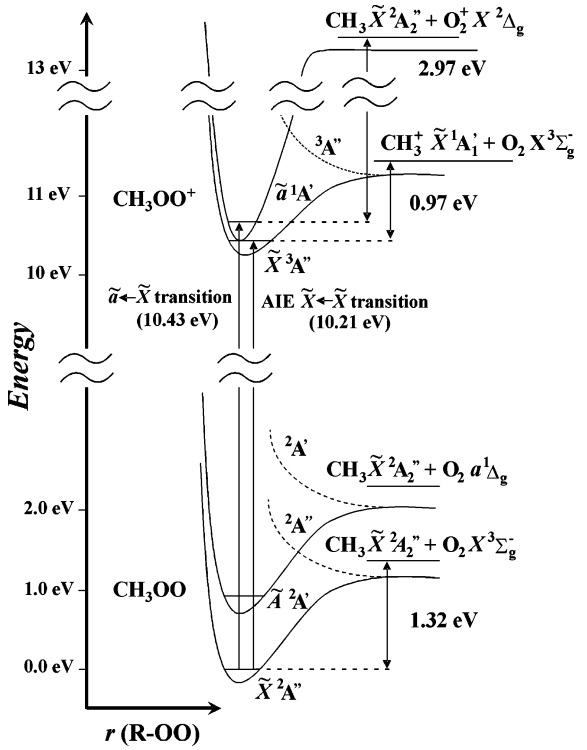

Figure 3. Schematic potential energy diagram of CH_3OO/CH_3OO^+ as derived from the CBS-APNO calculations.

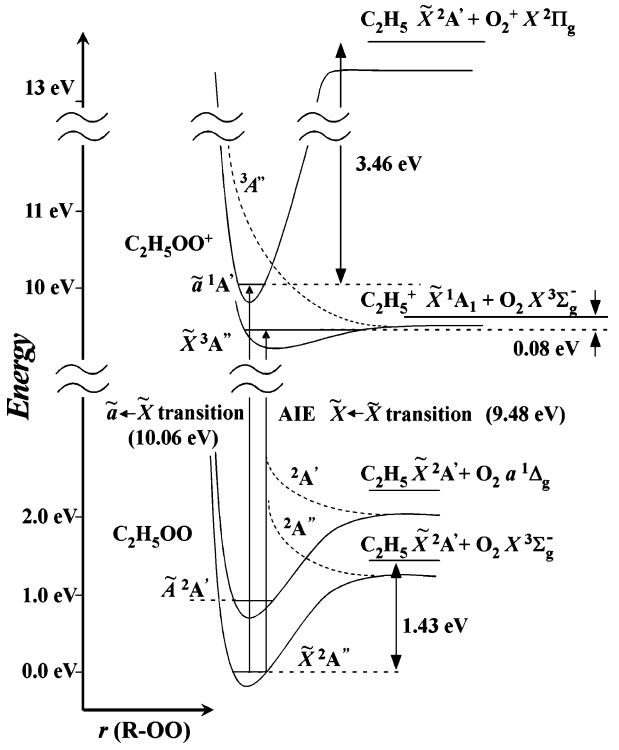

Figure 4. Schematic potential energy diagram of $C_2H_5OO/C_2H_5OO^+$ as derived from the CBS-APNO calculations.

The splitting between the singlet and triplet levels of the cation is calculated to be 0.12 eV by QCISD(T)/∞ and to be 0.22 eV by CBS/APNO. The value of the singlet−triplet splitting was varied in the fit (yielding a fitted value of 0.11 eV); however, fits that were constrained to either calculated splitting yielded adiabatic ionization energies that agreed to within 0.003 eV. The total estimated uncertainty derives from many considerations, including the 95% precision of the fit (±0.006 eV), the approximate nature of calculated Franck−Condon factors, the photon energy calibration, possible presence of hot bands, and field ionization of high-lying Rydberg states.

Because the experiment resolves the dependence of the ionization signal on both time and photon energy, the dissociative ionization of CH_3OO to CH_3^+ and O_2 can be distinguished from the direct ionization of CH_3. Figure 6 shows a 2D image of the time- and photon-energy-dependent $m/z = 15$ signal from photodissociation of acetone in the presence of (6.2×10^{15}) cm^{-3} O_2. The rapid disappearance of CH_3 radicals can be seen as the peak near $t = 0$ which is present at all photon energies in the figure. At higher photon energies, signal at $m/z = 15$ persists for longer times. This signal is attributable to dissociative ionization of CH_3OO. The appearance energy of CH_3^+ from CH_3OO is related to the ground-state bond energy and the ionization energy of CH_3:

$$\mathrm{AE}(CH_3^+,CH_3OO) = D_0^o(CH_3 - OO) + \mathrm{AIE}(CH_3) \quad (7)$$

Figure 7 shows the observed dissociative ionization signal at $m/z = 15$ as a function of photon energy. The dissociative ionization component is derived by integrating the observed $m/z = 15$ signal for times after the kinetic decay of the methyl radical is complete. A small background contribution remains after this

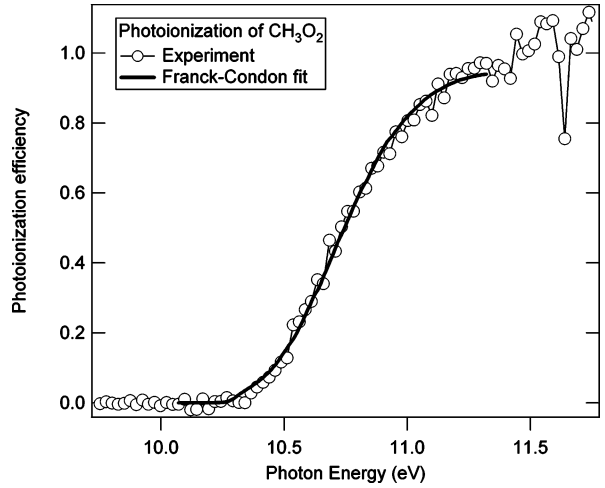

Figure 5. Franck−Condon calculated PIE curve (thick solid line) for CH_3OO is superimposed on the experimental PIE curves (open circles), taken with a 0.025 eV step size and 600 μm slit aperture (approximate energy resolution of 40 meV).

procedure, so the average of the signal at photon energies below 10.9 eV is subtracted to give the final estimate of the dissociative ionization signal. The threshold is fit using an exponential kernel function convolved with a 298 K energy distribution; the density-of-states function is approximated as that of a four-dimensional rotor, following Ruscic and Berkowitz.[47] The AE-(CH_3^+, CH_3OO) = (11.16 ± 0.05) eV is derived from the present experiments, where the estimated uncertainty includes the 95% precision limits of the fit (±0.034 eV), uncertainty in the photon energy calibration, and the approximate nature of the state density model. Combined with the AIE of CH_3, (9.8380 ± 0.0004) eV,[48] this appearance energy yields an experimental bond energy of $D_0^o(CH_3 - OO)$ = (127.6 ± 5) kJ mol^{-1}. Using the 0 K enthalpy of formation for CH_3,[49] $\Delta_f H_0^o(CH_3)$ = (150.0 ± 0.3) kJ mol^{-1}, this bond energy implies an enthalpy of formation for CH_3OO of $\Delta_f H_0^o(CH_3OO)$ = (22.4 ± 5) kJ mol^{-1}. The CBS-APNO value for the neutral C−O bond energy, $D_0^o(CH_3 - OO)$= 127.3 kJ mol^{-1}, and the corresponding QCISD(T)/∞ value, $D_0^o(CH_3 - OO)$ = 127.6 kJ mol^{-1}, are in excellent agreement with the experimental value. The derived enthalpy of formation for CH_3OO is slightly lower than that reported by Blanksby et al.,[24] whose value of $\Delta_f H_{298}^o(CH_3OO)$ = (20.1 ± 5) kJ mol^{-1} corresponds to $\Delta_f H_0^o(CH_3OO)$ = (30.1 ± 5) kJ mol^{-1}, but is in good agreement with the $\Delta_f H_0^o(CH_3OO)$ = (19.0 ± 5) kJ mol^{-1} obtained from the kinetic determinations of Knyazev and Slagle.[26] Because of the established thermochemistry[48,49] of CH_3 and CH_3^+, measurements of the dissociative ionization of CH_3OO in a supersonic beam,[32] perhaps by higher-resolution laser methods, may prove a means to high-precision determination of the bond energy of CH_3OO.

The enthalpy of formation of the CH_3OO^+ radical, $\Delta_f H_0^o(CH_3OO^+)$, can be determined using the adiabatic ionization energy and $\Delta_f H_0^o(CH_3OO)$ via the simple equation:

$$\Delta_f H_0^o(CH_3OO^+) = \Delta_f H_0^o(CH_3OO) + AIE \qquad (8)$$

Combining the values of (997 ± 5) kJ mol^{-1} for AIE(CH_3OO) and $\Delta_f H^o(CH_3OO)$ = (22.4 ± 5) kJ mol^{-1}, measured in this investigation, yields $\Delta_f H_0^o(CH_3OO^+)$ = (1019 ± 7) kJ mol^{-1}. This value is in reasonable agreement with the CBS-APNO-computed $\Delta_f H_0^o(CH_3OO^+)$ value of 1006 kJ mol^{-1} and in excellent agreement with the QCISD(T)/∞ value of 1019 kJ mol^{-1}, evaluated using relationship 8 and the calculated heats of formation and ionization energies.

From the enthalpies of formation of both CH_3OO^+ and CH_3^+, we can also extract the bond energy $D_0^o(CH_3^+ - OO)$ = (80 ± 7) kJ mol^{-1} using

$$D_0^o(CH_3^+ - OO) = \Delta_f H_0^o(CH_3^+) - \Delta_f H_0^o(CH_3OO^+) \qquad (9)$$

The experimentally derived $D_0^o(CH_3 - OO)$ and $D_0^o(CH_3^+ - OO)$ show that the neutral CH_3OO is 47.6 kJ mol^{-1} (0.49 eV) more stable than CH_3OO^+ with respect to the corresponding ground-state products, in agreement with the calculations. The C−O bond in the cation is weaker than that in the neutral because of the removal of one of the σ(C−O) bonding electrons upon photoionization.

C_2H_5OO. The C_2H_5OO PIE curve could not be measured because of the lack of parent $C_2H_5OO^+$ signal. However, from the time- and photon-energy-resolved mass spectra of m/z = 29 from the reaction of C_2H_5 with O_2, shown in Figure 8, it is clear there are two sources of $C_2H_5^+$. Just as in the case of CH_3^+ from photoionization measurements of the reaction of CH_3 with O_2, the observed $C_2H_5^+$ signal in the $C_2H_5 + O_2$ system quickly decays to the baseline level for photon energies below about 10 eV, reflecting the rapid removal of ethyl radicals by reaction with oxygen. At higher photon energies, however, m/z = 29 signal persists to long times. Under the present conditions, ethyl is completely converted to the stable ethylperoxy product within several milliseconds. After that time dissociative ionization of ethylperoxy produces an approximately constant amount of $C_2H_5^+$ proportional to the concentration of C_2H_5OO. At room temperature, thermal redissociation of ethylperoxy to ethyl + O_2 is negligible on the time scale of these experiments. The dissociative ionization contribution to the m/z = 29 signal is shown in Figure 9.

Further support that the $C_2H_5^+$ signal arises from dissociative ionization is given by the observed appearance energy (Figure 9) of ∼10 eV, substantially higher than the C_2H_5 adiabatic ionization energy of (8.117 ± 0.008) eV.[50] The fact that the $C_2H_5OO^+$ ion is not detected suggests that the peroxy cation is not bound, or only weakly bound, with respect to the ground-state products, $C_2H_5^+$ and O_2, in agreement with our computations (Figure 4).

$$C_2H_5OO + h\nu_{ALS} \rightarrow C_2H_5^+ + O_2 + e^- \qquad (10)$$

The appearance energy for the $C_2H_5^+$ fragment from the dissociative ionization process of ethylperoxy is related to

(47) Ruscic, B.; Berkowitz, J. *J. Phys. Chem* **1993**, *97*, 11451−11455.
(48) Blush, J. A.; Chen, P.; Wiedmann, R. T.; White, M. G. *J. Chem. Phys.* **1993**, *98*, 3557−3559.
(49) Ruscic, B.; Boggs, J. E.; Burcat, A.; Császár, A. G.; Demaison, J.; Janoschek, R.; Martin, J. M. L.; Morton, M. L.; Rossi, M. J.; Stanton, J. F.; Szalay, P. G.; Westmoreland, P. R.; Zabel, F.; Bérces, T. *J. Phys. Chem. Ref. Data* **2005**, *34*, 573−656.
(50) Ruscic, B.; Berkowitz, J.; Curtiss, L. A.; Pople, J. A. *J. Chem. Phys.* **1989**, *91*, 114−21.

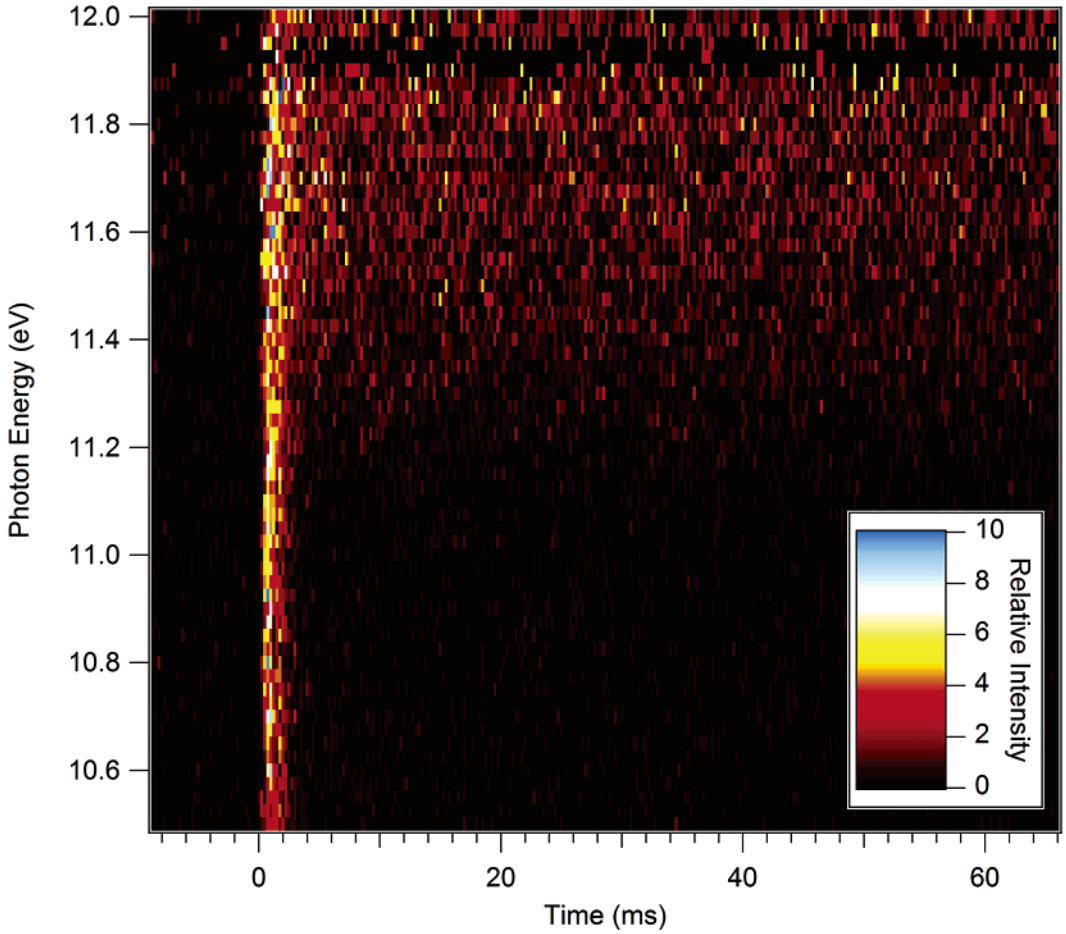

Figure 6. Time- and photon-energy-resolved measurements of CH_3^+ ($m/z = 15$) photoionization signal following photolysis of acetone in the presence of O_2. The time is measured relative to the photolysis pulse. Direct ionization of methyl radicals gives a peak near time zero, which decays rapidly as the reaction with O_2 proceeds. This process is visible for photoionization energies above 9.84 eV (the AIE of CH_3) and results in the strong vertical stripe in the figure. The signal at longer times that appears only for high photon energies is attributable to dissociative ionization of CH_3OO.

the AIE of the ethyl radical and the neutral bond energy via the expression

$$\mathrm{AE}(\mathrm{C_2H_5}^+,\mathrm{C_2H_5OO}) = D_0^{\circ}(\mathrm{C_2H_5} - \mathrm{OO}) + \mathrm{AIE}(\mathrm{C_2H_5}) \quad (11)$$

Using the $D_0^{\circ}(C_2H_5 - OO)$ of (144.2 ± 7.8) kJ mol^{-1} ((1.49 ± 0.08) eV) derived from reported enthalpies of formation of C_2H_5OO [24] and C_2H_5, and AIE(C_2H_5), the AE($C_2H_5^+$, C_2H_5OO) is predicted to be (9.61 ± 0.08) eV. This value is much lower than the observed appearance energy of $C_2H_5^+$. A likely interpretation of this apparent discrepancy is that the observed $C_2H_5^+$ fragment derives from dissociative ionization occurring through the $\tilde{a}^1A'$ state of $C_2H_5OO^+$ via curve-crossing to a $^3A''$ repulsive state correlating with $C_2H_5^+$ ($\tilde{X}^1A_1$) + O_2 ($X\ ^3\Sigma_g^-$). In fact, ionization to $C_2H_5OO^+$ in its $^3A''$ ground state should be very weak due to poor Franck−Condon overlap (see Figure 4 and Table 2). Direct ionization to the ground state of the $C_2H_5OO^+$ (which is expected to be at best weakly bound based on the present calculations) may be below the signal-to-noise of the present experiments. However, more favorable Franck−Condon factors are expected for the $C_2H_5OO^+$ ($\tilde{a}^1A'$) + e^- ← C_2H_5OO ($\tilde{X}^2A''$) transition. The adiabatic energy for the $\tilde{a} \leftarrow \tilde{X}$ transition is calculated to be 10.06 eV at the CBS-APNO method, which is in reasonable agreement with the experimentally observed 298 K appearance threshold of (10.0 ± 0.1) eV. Under this interpretation the dissociative ionization

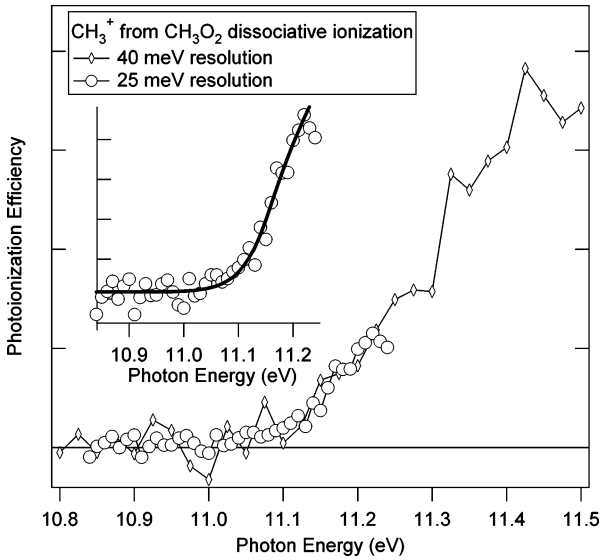

Figure 7. Measurements of CH_3^+ ($m/z = 15$) derived from dissociative ionization of CH_3OO, taken at two photon energy resolutions. The inset shows a fit near the threshold, using an exponential kernel function convolved with a 298 K energy distribution, which yields a 0 K appearance energy of (11.16 ± 0.05) eV.

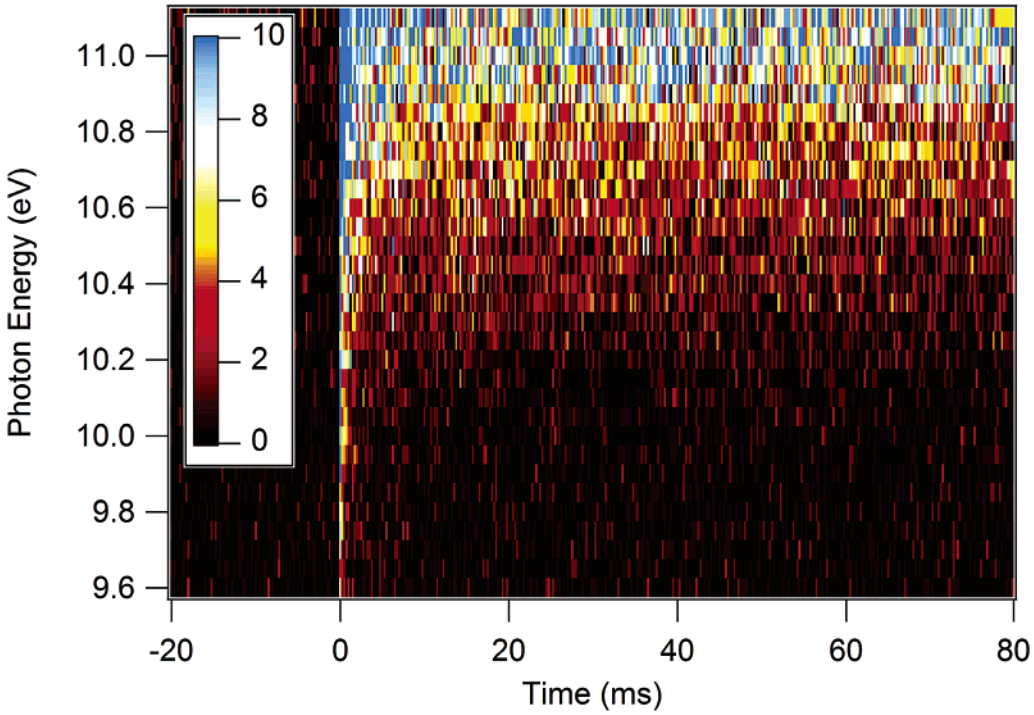

Figure 8. Time- and photon-energy-resolved measurements of $C_2H_5^+$ ($m/z = 29$) photoionization signal following photolysis of 3-pentanone in the presence of O_2. The contributions of direct ionization of ethyl radicals and the dissociative ionization of C_2H_5OO are clearly visible (cf. Figure 6).

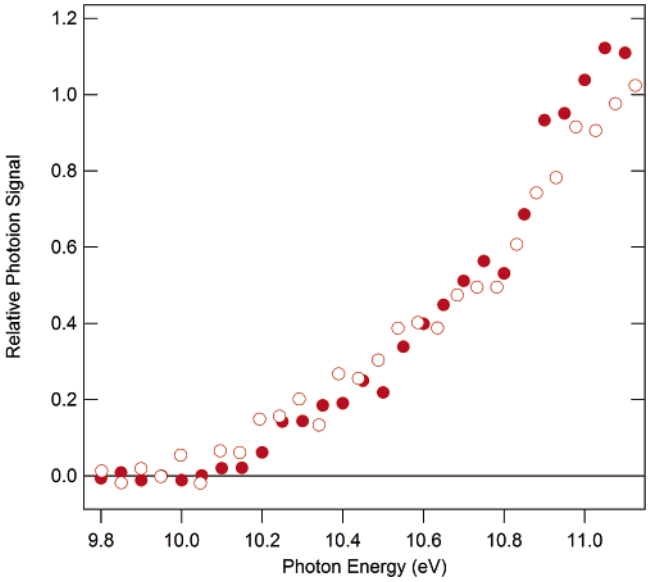

Figure 9. Measurements of $C_2H_5^+$ ($m/z = 29$) photoionization signal from dissociative ionization of C_2H_5OO, taken with a 0.050 eV step size and 1 mm slit aperture.

relies on coupling between the bound singlet state and unbound levels in the triplet manifold. In this case the photoelectron spectrum may bear the signature of the singlet cation state. Furthermore, it is conceivable that rapid pump−probe experiments could interrogate the singlet cation before intersystem crossing and dissociation occur.

Preliminary experiments on the photoionization of *n*-propylperoxy radical, C_3H_7OO, show that the parent cation is not detectable, just as for ethylperoxy. The $C_3H_7^+$ signal from dissociative ionization of C_3H_7OO has been detected. More experiments are planned to investigate the stability of larger ROO^+ radicals, and such results will be presented in a future publication. The present results suggest that among the linear alkylperoxy radicals only CH_3OO^+ is bound with respect to the ground-state products CH_3^+ and O_2. Ethylperoxy and propylperoxy radicals dissociatively ionize to produce alkyl cations and molecular oxygen.

The most striking difference between CH_3OO and the larger alkylperoxy radicals is the dramatic reduction in C−O bond strength in the cations from $(D_0^o(CH_3^+ - OO) = (80 \pm 7)$ kJ mol^{-1} to $D_0^o(R^+ - OO) \cong 0$ in the ethyl- and propylperoxy cations. Examination of the electronic structure of peroxy radicals and their cations can explain the instability of the larger peroxy cations. The lowest-energy ionization of the neutral radicals in all cases removes an electron from the $\sigma(C_\alpha-O)$ orbital of a′ symmetry, creating the $^3A''$ ground state of the cation with one electron remaining in this orbital. The removal of one bonding electron leads to a substantial lengthening of the C−O bond in the cation, as shown in Table 2, and a concomitant decrease of the C−O bond strength in the cation as compared to the neutral. In addition to this effect, the further reduction in the C−O bond strengths in the ethyl- and propylperoxy cations can be partially rationalized as being a result of hyperconjugation that is not possible in CH_3OO^+.

The relative instability of $C_2H_5OO^+$ can also be viewed as reflecting the stability of the fragment $C_2H_5^+$ ion. Hyperconjugation of the $\sigma(C_\beta-H)$ orbital with the empty $p(C_\alpha)$ orbital stabilizes the ethyl cation, and similar hyperconjugation provides increasing stabilization of more highly substituted carbocations.[51,52] A remnant of this hyperconjugation is preserved in the $C_2H_5OO^+$ ion, where electron density from the doubly occupied $\sigma(C_\beta-H)$ orbital of a′ symmetry (lying in the C−C−O−O plane) is donated, but now to the $\sigma^*(C_\alpha-O)$ orbital

(51) Muller, N.; Mulliken, R. S. *J. Am. Chem. Soc* **1958**, *80*, 3489−3497.
(52) Radom, L.; Pople, J. A.; Schleyer, P. v. R. *J. Am. Chem. Soc* **1972**, *94*, 5935−5945.

that corresponds to the $p(C_\alpha)$ orbital of $C_2H_5^+$. As a result of this π-bonding interaction the $C_\alpha-C_\beta$ bond strengthens and shortens, while the donor $C_\beta-H$ bond weakens and lengthens somewhat. Additionally, the C−O bond lengthens to the point that it is either very weak or nonexistent. The geometry changes implied by this valence bond description are supported by the calculated geometries in Table 2. Hyperconjugation has also been invoked to explain C−O bond enthalpies in neutral alkylperoxy radicals.[53]

The C−O bond in CH_3OO^+ is weakened from that in the neutral simply because of the removal of one electron from the $\sigma(C_\alpha-O)$ bonding orbital. However, without the additional weakening of the bond (or stabilization of the methyl cation) by hyperconjugation, the CH_3OO^+ cation is stable. On the other hand, alkylperoxy radicals of secondary or tertiary alkyl radicals are even less likely to have stable cations than ethylperoxy. Substituent effects on hyperconjugation and carbocation stability have been extensively investigated; it might be expected that alkyl cations with hyperconjugative stabilization equal to or larger than that of the ethyl cation will not form stable bonds with O_2. Investigation of substituent effects on alkylperoxy photoionization will illuminate the role of hyperconjugation in the thermochemistry of these systems.

Conclusions

A new experimental apparatus that combines the tunability of the VUV radiation of the ALS at Lawrence Berkeley National Laboratory with a time- and photon-energy-resolved mass spectrometer has been used to investigate the ionization of simple linear alkylperoxy radicals.

The photoionization efficiency curve for CH_3OO^+ has been recorded for the first time, and an adiabatic ionization energy of (10.33 ± 0.05) eV has been measured with the aid of Franck−Condon spectral simulations. From this value and the appearance energy of CH_3^+, the enthalpies of formation $\Delta_f H_0^o(CH_3OO) = (22.4 \pm 5)$ kJ mol^{-1} and $\Delta_f H_0^o(CH_3OO^+) = (1019 \pm 7)$ kJ mol^{-1} have been derived. The $CH_3^+ - OO$ bond energy of (80 ± 7) kJ mol^{-1} is then obtained. From ethylperoxy radicals the $C_2H_5OO^+$ signal is not detectable, and thus the $C_2H_5OO^+$ PIE curve is not recorded. Electronic structure calculations show that the $C_2H_5OO^+$ radical is at most only slightly bound with respect to the ground-state products, $C_2H_5^+$ and O_2. The time behavior of the observed $C_2H_5^+$ signal from photoionization of the products of the $C_2H_5 + O_2$ reaction demonstrates its formation from the dissociative ionization of $C_2H_5OO^+$. Hyperconjugation reduces the stability of the ethylperoxy cation, making the $C_2H_5OO^+$ ground state only slightly bound, or unbound, with respect to the ground-state fragments $C_2H_5^+$ and O_2. This destabilizing effect will make it difficult to detect the parent cations of all larger alkylperoxy radicals.

Acknowledgment. We acknowledge Prof. Vadim Knyazev (Catholic University of America); Prof. Simon North (Texas A&M University); Dr. Darcy Peterka, Dr. Kevin Wilson, and Dr. Christophe Nicolas (Lawrence Berkeley National Laboratory); Dr. Carl Hayden and Mr. Howard Johnsen (Sandia National Laboratories) for their many contributions toward successful operation of this new apparatus; and Prof. Barry Carpenter (Cornell University) for bringing to our attention the possibility of hyperconjugation effects in alkylperoxy cations. This work is supported by the Division of Chemical Sciences, Geosciences, and Biosciences, the Office of Basic Energy Sciences, the United States Department of Energy. The work at Argonne was supported under DOE Contract Number W-31-109-ENG-38. Sandia is a multiprogram laboratory operated by Sandia Corporation, a Lockheed Martin Company, for the National Nuclear Security Administration under contract DE-AC04-94-AL85000. The Advanced Light Source is supported by the Director, Office of Science, Office of Basic Energy Sciences, Materials Sciences Division, of the United States Department of Energy under Contract No. DE-AC02-05CH11231 at Lawrence Berkeley National Laboratory.

Supporting Information Available: Complete ref 36. This material is available free of charge via the Internet at http://pubs.acs.org.

JA064556J

(53) Pratt, D. A.; Porter, N. A. *Org. Lett.* **2003**, *5*, 387−390.